

Development of a non-equilibrium gas flow capability within *Code_Saturne* using the Method of Moments

Xiaojun Gu, Charles Moulinec and David R. Emerson

Scientific Computing Department,
STFC Daresbury Laboratory, Warrington WA4 4AD



1. Introduction

Non-equilibrium gas flows represent a fundamental modelling challenge and exist in many industrial applications and scientific research facilities, including mass spectrometry, low-pressure environments, vacuum pumps, micro-electro-mechanical systems (MEMS), high-altitude vehicles, and porous media. The extent of the non-equilibrium state is usually measured by the Knudsen number, Kn , which is the ratio of the gas molecular mean free path to the characteristic macroscopic length scale of the flow. If the Knudsen number is very small ($Kn < 0.001$), continuum theory is considered to be valid and the no-slip boundary condition can be applied i.e. the Navier-Stokes-Fourier (NSF) equations can be used in the prediction of flow fields. When the Knudsen number lies in the range $0.001 < Kn < 0.1$, the flow is in the slip regime and the NSF equations can only be used if the wall boundary conditions are modified to account for velocity-slip and temperature-jump. For $0.1 < Kn < 10$, the flow enters the transition regime and the NSF equations are no longer able to predict the flow field with any degree of accuracy. Kinetic theory approaches, such as the Boltzmann equation or direct simulation Monte Carlo (DSMC), can be used in this regime. For the Boltzmann equation, the complexity of the collision term makes it difficult to use in all but simple problems. In the case of DSMC, the computational cost is prohibitive and, apart from flow with high Kn , simulations are limited to 2-D and low-speed problems can take weeks to solve. When $Kn > 10$, the flow is in the free-molecular regime and molecular collisions can be ignored. Without collisions, kinetic methods offer a computationally efficient approach. However, in the early transition regime ($0.1 < Kn < 1$), the moment method offers the best approach for capturing rarefied phenomena. More physics is embedded in the moment equations than in the NSF equations with only a modest increase in computational cost.

We have successfully demonstrated that the moment equations can be used to study a range of classic problems including Couette flow, Poiseuille flow, and Kramers' problem which have all been studied theoretically (Gu *et al* 2010; Gu & Emerson 2014). Numerical investigations of 2-D driven cavity flow (Gu *et al* 2009) and flow past a circular cylinder (Gu *et al* 2019) have demonstrated that the Method of Moments has great potential. However, there is currently no software available that can solve non-equilibrium flows in the early transition regime ($0.1 < Kn < 1$) in 3-D complex geometries with a computational efficiency similar to conventional Computational Fluid Dynamics (CFD) problems. An understanding of the flow in the transition regime is essential to design, predict, and operate a wide range of practical devices. It is now timely and beneficial to develop software which will bridge the gap between the continuum approach and kinetic theory. The open-source CFD software, *Code_Saturne* (<https://www.code-saturne.org/cms/>), which performs well on ARCHER, provides a well-defined and flexible platform to solve the moment equations. It already has a wide and growing range of academic and industrial users and this enhancement will expand its capability into a new research and industrial dimension by developing and implementing a rarefied gas dynamics module with the moment equations.

2. Extended thermodynamic governing equations

2.1. Conventional hydrodynamic model - the NSF equations

The traditional hydrodynamic quantities of density, ρ , velocity, u_i , and temperature, T , correspond to the first five lowest-order moments of the molecular distribution function. The governing equations of these hydrodynamic quantities for a dilute gas can be obtained from the Boltzmann equation and represent mass, momentum, and energy conservation laws, respectively (Struchtrup 2005):

$$\frac{\partial \rho}{\partial t} + \frac{\partial \rho u_i}{\partial x_i} = 0, \quad (1)$$

$$\frac{\partial \rho u_i}{\partial t} + \frac{\partial \rho u_i u_j}{\partial x_j} + \frac{\partial \sigma_{ij}}{\partial x_j} = - \frac{\partial p}{\partial x_i}, \quad (2)$$

and

$$\frac{\partial \rho T}{\partial t} + \frac{\partial \rho u_i T}{\partial x_i} + \frac{2}{3R} \frac{\partial q_i}{\partial x_i} = -\frac{2}{3R} \left(p \frac{\partial u_i}{\partial x_i} + \sigma_{ij} \frac{\partial u_j}{\partial x_i} \right), \quad (3)$$

where t and x_i are the temporal and spatial coordinates, respectively, and any suffix i, j, k represents the usual summation convention. The pressure, p , is related to the temperature and density by the ideal gas law, $p = \rho RT$, where R is the specific gas constant. However, the stress term, σ_{ij} , and heat flux term, q_i , given in equations (2) and (3) are unknown. The classical way to close this set of equations is through a Chapman-Enskog (CE) expansion of the molecular distribution function in terms of Kn around the Maxwellian which is first-order in Hermite polynomials. The zeroth-order CE expansion yields the Euler equations and the first-order approximation of σ_{ij} and q_i , for Maxwell molecules, gives (Chapman & Cowling 1970, Struchtrup 2005):

$$\sigma_{ij}^G = -2\mu \frac{\partial u_{<i}}{\partial x_{j>}} \quad \text{and} \quad q_i^G = -\frac{15}{4} R\mu \frac{\partial T}{\partial x_i}, \quad (4)$$

in which μ is the viscosity and the angular brackets denote the traceless part of a symmetric tensor. Equation (4) expresses an important transport mechanism for u_i and T : the gradient transport mechanism and the superscript G is used to emphasise its importance. Let

$$\sigma_{ij} = \sigma_{ij}^G \quad \text{and} \quad q_i = q_i^G \quad (5)$$

and insert equations (4) and (5) into equations (2) and (3) results in the traditional hydrodynamic equations.

2.2. A second moment closure model - the R13 equations

As the value of Kn increases, more moments are needed to accurately describe any non-equilibrium phenomena. Grad (1949) truncated the distribution function to the incomplete third-order in Hermite polynomials (f_{G13}). Grad was one of the pioneers to introduce σ_{ij} and q_i as extended variables and derived a set of governing equations for them from the Boltzmann equation. For Maxwell molecules, the stress and heat flux equations are (Struchtrup 2005):

$$\frac{\partial \sigma_{ij}}{\partial t} + \frac{\partial u_k \sigma_{ij}}{\partial x_k} + \frac{\partial m_{ijk}}{\partial x_k} = -A_\sigma \frac{p}{\mu} \sigma_{ij} - 2p \frac{\partial u_{<i}}{\partial x_{j>}} + \Sigma_{ij}, \quad (6)$$

and

$$\frac{\partial q_i}{\partial t} + \frac{\partial u_j q_i}{\partial x_j} + \frac{1}{2} \frac{\partial R_{ij}}{\partial x_j} = -A_q \frac{p}{\mu} q_i - \frac{5}{2} pR \frac{\partial T}{\partial x_i} + Q_i, \quad (7)$$

in which

$$\Sigma_{ij} = -\frac{4}{5} \frac{\partial q_{<i}}{\partial x_{j>}} - 2\sigma_{k<i} \frac{\partial u_{j>}}{\partial x_k} \quad (8)$$

and

$$Q_i = -\frac{7\sigma_{ik}R}{2} \frac{\partial T}{\partial x_k} - RT \frac{\partial \sigma_{ik}}{\partial x_k} + \frac{\sigma_{ij}}{\rho} \left(\frac{\partial p}{\partial x_j} + \frac{\partial \sigma_{jk}}{\partial x_k} \right) - \frac{2}{5} \left(\frac{7}{2} q_k \frac{\partial u_i}{\partial x_k} + q_k \frac{\partial u_k}{\partial x_i} + q_i \frac{\partial u_k}{\partial x_k} \right) - \frac{1}{6} \frac{\partial \Delta}{\partial x_i} - m_{ijk} \frac{\partial u_j}{\partial x_k}. \quad (9)$$

Here, m_{ijk} , R_{ij} and Δ represent the difference between the true value of the higher moments and their approximated value with f_{G13} . In Grad's original method, such deviations were not introduced, so that $m_{ijk} = R_{ij} = \Delta = 0$ which results in the well-known G13 equations. To close the set of equations, (1)-(3), (6) and (7), Struchtrup & Torrilhon (2003) and Struchtrup (2005) regularised the G13 equations and obtained the following closures:

$$m_{ijk} = -\frac{3\mu}{A_m \rho} \frac{\partial \sigma_{<ij}}{\partial x_{k>}} + \frac{3\mu}{A_m p} \left[\frac{\sigma_{<ij}}{\rho} \left(\frac{\partial p}{\partial x_{k>}} + \frac{\partial \sigma_{k>l}}{\partial x_l} \right) - \frac{4}{5} q_{<i} \frac{\partial u_j}{\partial x_{k>}} - \sigma_{<ij} \frac{\partial RT}{\partial x_{k>}} \right] \quad (10)$$

$$R_{ij} = -\frac{28}{5A_{R1}} \frac{\mu}{\rho} \frac{\partial q_{<i}}{\partial x_{j>}} - \frac{28}{5A_{R1}} \frac{\mu}{p} \left[2q_{<i} \frac{\partial RT}{\partial x_{j>}} - \frac{q_{<i}}{\rho} \left(\frac{\partial p}{\partial x_{j>}} + \frac{\partial \sigma_{j>k}}{\partial x_k} \right) - \frac{5}{6} \frac{\sigma_{ij}}{\rho} \left(\frac{\partial q_k}{\partial x_k} + \sigma_{kl} \frac{\partial u_k}{\partial x_l} \right) \right] \quad (11)$$

$$+ \frac{5RT}{7} \left(\sigma_{k<i} \frac{\partial u_{j>}}{\partial x_k} + \sigma_{k<i} \frac{\partial u_k}{\partial x_{j>}} - \frac{2}{3} \sigma_{ij} \frac{\partial u_k}{\partial x_k} \right) - \frac{A_{R2}}{A_{R1}} \frac{\sigma_{k<i} \sigma_{j>k}}{\rho}$$

and

$$\Delta = -\frac{8}{A_{\Delta 1}} \frac{\mu}{p} \left[\frac{7}{2} q_k \frac{\partial RT}{\partial x_k} - \frac{q_j}{\rho} \left(\frac{\partial p}{\partial x_j} + \frac{\partial \sigma_{jk}}{\partial x_k} \right) + RT \left(\frac{\partial q_k}{\partial x_k} + \sigma_{ij} \frac{\partial u_i}{\partial x_j} \right) \right] - \frac{A_{\Delta 2}}{A_{\Delta 1}} \frac{\sigma_{ij} \sigma_{ij}}{\rho}. \quad (12)$$

Struchtrup (2005) denoted this set of 13 moment equations with the above closure as the R13 equations.

2.3. Extending the hydrodynamic model- the R26 equations

It was found (Gu *et al.* 2010; Young 2011; Gu & Emerson 2014) that the R13 are not adequate enough to capture the Knudsen layer in Kramers' problem and the regularised 26 moment equations (R26) are required to accurately reproduce the velocity defect found with kinetic data. However, both the R13 and R26 equations are able to capture many of the non-equilibrium phenomena observed using kinetic theory. These include effects such as the tangential heat flux in planar Couette flow and the bimodal temperature profile in planar force-driven Poiseuille flow (Taheri & Struchtrup 2009; Taheri *et al.* 2009; Gu & Emerson 2007, 2009). Since equations (10) and (11) are algebraic approximations for m_{ijk} and R_{ij} , they have no mechanism to produce a boundary layer for themselves near the wall. Alternatively, the governing equations of m_{ijk} , R_{ij} and Δ derived from the Boltzmann equation can be used to provide information required in equations (6) and (7). They are (Gu & Emerson 2009):

$$\frac{\partial m_{ijk}}{\partial t} + \frac{\partial u_l m_{ijk}}{\partial x_l} + \frac{\partial \phi_{ijkl}}{\partial x_i} = -A_m \frac{p}{\mu} m_{ijk} - 3RT \frac{\partial \sigma_{<ij}}{\partial x_{k>}} - \frac{3}{7} \frac{\partial R_{<ij}}{\partial x_{k>}} + M_{ijk}, \quad (13)$$

$$\frac{\partial R_{ij}}{\partial t} + \frac{\partial u_k R_{ij}}{\partial x_k} + \frac{\partial \psi_{ijk}}{\partial x_k} = -A_{R1} \frac{p}{\mu} R_{ij} - \frac{28}{5} RT \frac{\partial q_{<i}}{\partial x_{j>}} - 2RT \frac{\partial m_{ijk}}{\partial x_k} - \frac{2}{5} \frac{\partial \Omega_{<i}}{\partial x_{j>}} + \mathfrak{R}_{ij} \quad (14)$$

and

$$\frac{\partial \Delta}{\partial t} + \frac{\partial \Delta u_i}{\partial x_i} + \frac{\partial \Omega_i}{\partial x_i} = -A_{\Delta 1} \frac{p}{\mu} \Delta - 8RT \frac{\partial q_k}{\partial x_k} + \aleph, \quad (15)$$

in which, M_{ijk} , \mathfrak{R}_{ij} and \aleph are the nonlinear source terms (Gu & Emerson 2009). Here, ϕ_{ijkl} , ψ_{ijk} and Ω_i are the difference between the true value of the higher moments and their approximated value with f_{G26} . In the R26 equations (Gu & Emerson 2009), they were obtained by a Chapman-Enskog expansion. For convenience, they can be expressed as gradient transport terms and the high-order nonlinear terms, respectively, by

$$\left\{ \begin{array}{l} \phi_{ijkl} = -\frac{4\mu}{A_{\phi 1} \rho} \frac{\partial m_{<ijk}}{\partial x_{l>}} + \phi_{ijkl}^{NL}, \\ \psi_{ijk} = -\frac{27\mu}{7A_{\psi 1} \rho} \frac{\partial R_{<ij}}{\partial x_{k>}} + \psi_{ijk}^{NL}, \\ \Omega_i = -\frac{7}{3} \frac{\mu}{A_{\Omega} \rho} \frac{\partial \Delta}{\partial x_i} - 4 \frac{\mu}{A_{\Omega} \rho} \frac{\partial R_{ik}}{\partial x_k} + \Omega_i^{NL}, \end{array} \right. \quad (16)$$

Here ϕ_{ijkl}^{NL} , ψ_{ijk}^{NL} and Ω_i^{NL} are the remaining nonlinear terms of ϕ_{ijkl} , ψ_{ijk} and Ω_i , respectively, and are provided by Gu and Emerson (2009). The values of the collision constants, A_σ , A_q , A_m , A_{R1} , A_{R2} , $A_{\Delta1}$, $A_{\Delta2}$, A_ϕ , A_ψ and A_Ω , depend on the molecular collision model adopted and represent the relaxation time-scale for each moment. They are given in Table 1 for the case of Maxwell molecules (Truesdell & Muncaster 1980; Struchtrup 2005), as employed in the present study. Although a dilute monatomic gas is employed, all the findings in the present study have relevance to realistic gases, such as air.

A_σ	A_q	A_m	A_{R1}	A_{R2}	$A_{\Delta1}$	$A_{\Delta2}$	A_ϕ	A_ψ	A_Ω
1.0	2/3	3/2	7/6	2/3	2/3	2/3	2.097	1.698	1.0

TABLE 1. Collision constants in the moment equations for Maxwell molecules

3. Wall boundary conditions

To apply any of the foregoing models to flows in confined geometries, appropriate wall boundary conditions are required to determine a unique solution. Gu & Emerson (2009) obtained a set of wall boundary conditions for the R26 equations based on Maxwell's kinetic wall boundary condition (Maxwell 1879) and a fifth-order approximation of the molecular distribution function in Hermite polynomials. In a frame where the coordinates are attached to the wall, with n_i the normal vector out of the wall pointing towards the gas and τ_i the tangential vector of the wall, the slip velocity parallel to the wall, u_τ , and temperature-jump conditions are:

$$u_\tau = -\frac{2-\alpha}{\alpha} \sqrt{\frac{\pi RT}{2}} \frac{\sigma_{n\tau}}{p_\alpha} - \frac{q_\tau}{5p_\alpha} - \frac{m_{n\tau}}{2p_\alpha} + \frac{9\Omega_\tau + 70\psi_{n\tau}}{2520p_\alpha RT} \quad (17)$$

and

$$RT - RT_w = -\frac{2-\alpha}{\alpha} \sqrt{\frac{\pi RT}{2}} \frac{q_n}{2p_\alpha} - \frac{RT\sigma_{nn}}{4p_\alpha} + \frac{u_\tau^2}{4} - \frac{75R_{nn} + 28\Delta}{840p_\alpha} + \frac{\phi_{nnnn}}{24p_\alpha} \quad (18)$$

where

$$p_\alpha = p + \frac{\sigma_{nn}}{2} - \frac{30R_{nn} + 7\Delta}{840RT} - \frac{\phi_{nnnn}}{24RT} \quad (19)$$

Here σ_{nn} , $\sigma_{n\tau}$, q_τ , $m_{n\tau}$, m_{nnn} , R_{nn} , $\psi_{n\tau}$, Ω_τ and ϕ_{nnnn} are the tangential and normal components of σ_{ij} , q_i , m_{ijk} , R_{ij} , ψ_{ijk} , Ω_i and ϕ_{ijkl} relative to the wall, respectively. It should be noted that the normal velocity at the wall, $u_n = 0$, since there is no gas flow through the wall. The accommodation coefficient, α , represents the fraction of gas molecules which will be *diffusively* reflected with a Maxwellian distribution at the temperature of the wall, T_w . The remaining fraction $(1-\alpha)$ of gas molecules will undergo *specular* reflection. The rest of the wall boundary conditions are listed in Appendix C of Gu & Emerson (2009). Equations (17) and (18) are similar to the velocity-slip and temperature-jump conditions for the NSF equations (Cercignani 1975; Gad-el-Hak 1999) with the additional underlined terms on the right hand side providing the higher-order moment contributions which are not available in the NSF model. However, these higher-order moment terms can be used to derive a second-order slip boundary condition for the NSF equations (Taheri & Struchtrup 2010). The solution of the NSF equations in the present study is associated with the wall boundary conditions (17) and (18) without the underlined terms.

4. Module implementation

A module containing four sets of equations of different complexity was developed for *Code_Saturne* without alteration of the core code. In the current implementation, the user subroutine facility provided by *Code_Saturne* was used to incorporate the modules into *Code_Saturne*. All the

added subroutines were written in Fortran 90. The newly developed module will be merged into the core code in collaboration with the development team of *Code_Saturne* in EDF. All the subroutines have been transferred to the EDF *Code_Saturne* team.

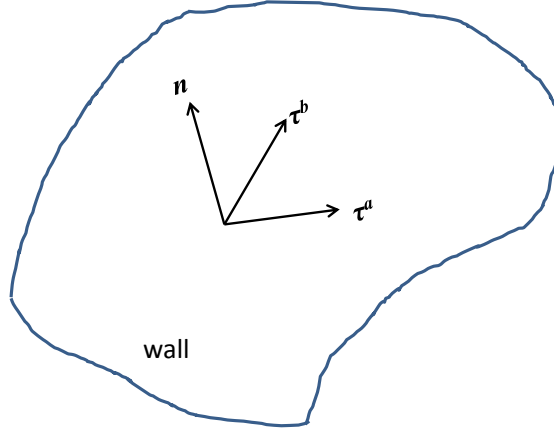


Figure 1 Orientation of a solid wall

4.1 NSF with velocity-slip and temperature-jump wall boundary conditions

Boundary arrays of “gas_velocity_slip” and “gas_temperature_jump” are created in the subroutine “cs_user_parameters_base.c”. The wall orientation is determined by the normal and tangential tensors, \mathbf{n} , $\boldsymbol{\tau}^a$ and $\boldsymbol{\tau}^b$, respectively. They are calculated, along with stresses and heat fluxes, in the subroutine “cs_user_boundary_conditions.f90”. The wall normal tensor, \mathbf{n} , is determined by the geometry and its components $\{n_x, n_y, n_z\}$ are provided by *Code_Saturne*. The tangential tensor, $\boldsymbol{\tau}^a$, is parallel to the slip velocity. Its components are determined by the corresponding components of the slip velocity as

$$\left(\tau_x^a, \tau_y^a, \tau_z^a\right) = \frac{(u_\tau, v_\tau, w_\tau)}{\sqrt{u_\tau^2 + v_\tau^2 + w_\tau^2}}. \quad (20)$$

The tangential tensor, $\boldsymbol{\tau}^b$, is then calculated by $\boldsymbol{\tau}^b = \mathbf{n} \times \boldsymbol{\tau}^a$.

Boundary arrays of “gas_velocity_slip” and “gas_temperature_jump” are evaluated by the wall boundary conditions (17) and (18) without the underlined terms in the subroutine “cs_user_boundary_conditions.f90”. They are set as Dirichlet boundary conditions for velocity and temperature equations. The components of the slip velocity are calculated from the stresses and heat fluxes by

$$u_\tau = -\frac{2 - \alpha}{\alpha} \frac{\sqrt{\pi RT}}{2} \frac{\left\{ n_x \left[\sigma_{xx} - (n_x^2 \sigma_{xx} + n_y^2 \sigma_{yy} + n_z^2 \sigma_{zz}) - 2n_y n_z \sigma_{yz} \right] + (1 - 2n_x^2) (n_y \sigma_{xy} + n_z \sigma_{xz}) \right\}}{p_\alpha} - \frac{\left\{ q_x - (n_x q_x + n_y q_y + n_z q_z) n_x \right\}}{5p_\alpha} \quad (21)$$

$$v_\tau = -\frac{2 - \alpha}{\alpha} \frac{\sqrt{\pi RT}}{2} \frac{\left\{ n_y \left[\sigma_{yy} - (n_x^2 \sigma_{xx} + n_y^2 \sigma_{yy} + n_z^2 \sigma_{zz}) - 2n_x n_z \sigma_{xz} \right] + (1 - 2n_y^2) (n_x \sigma_{xy} + n_z \sigma_{yz}) \right\}}{p_\alpha} - \frac{\left\{ q_y - (n_x q_x + n_y q_y + n_z q_z) n_y \right\}}{5p_\alpha} \quad (22)$$

$$w_\tau = -\frac{2-\alpha}{\alpha} \sqrt{\frac{\pi RT}{2}} \frac{\left\{ n_z \left[\sigma_{zz} - (n_x^2 \sigma_{xx} + n_y^2 \sigma_{yy} + n_z^2 \sigma_{zz}) - 2n_x n_y \sigma_{xy} \right] + (1-2n_z^2) (n_x \sigma_{xz} + n_y \sigma_{yz}) \right\}}{P_\alpha} - \frac{\left\{ q_z - (n_x q_x + n_y q_y + n_z q_z) n_z \right\}}{5p_\alpha} \quad (23)$$

4.2 Moment equations and their wall boundary conditions

Users are able to solve additional scalar convection and diffusion equations with sources within the user subroutine facility in *Code_Saturne*. This functionality of the code is used to implement the moment equations. Although the moments are tensors of different ranks, the individual Cartesian component of each tensor can be treated as a scalar, Φ . Both cell centre and boundary arrays of all the added variables are created in the subroutine “cs_user_parameters_base.c”. Arrays of derivatives are created in the subroutine “cs_usr_modules.f90”. Additional subroutines are created to calculate the source terms for the moment equations inside “cs_usr_modules.f90”. These source terms are fed into the solver through the subroutine “cs_user_source_terms.f90”. The wall boundary conditions are implemented in the subroutine “cs_user_boundary_conditions.f90”. To calculate the boundary value accurately, the derivatives of variables on the wall are required. However, *Code_Saturne* only calculates the derivatives at the cell centre. There is no straightforward way to calculate the derivatives on the wall in general. They are approximated by the values at the cell adjacent to the wall. This may lose some accuracy of the solution, particularly when the wall surface is complicated. To reduce any possible inaccuracy, a fine structured mesh with regular cells close to the wall is desirable.

The added primary variables for the various cases are, respectively,

$$\Phi = \begin{bmatrix} \sigma_{xx}, \sigma_{yy}, \sigma_{xy}, \sigma_{xz}, \sigma_{yz}, \\ q_x, q_y, q_z \end{bmatrix} \subset \text{R13 part}, \quad (24)$$

$$\Phi = \begin{bmatrix} \sigma_{xx}, \sigma_{yy}, \sigma_{xy}, \sigma_{xz}, \sigma_{yz}, \\ q_x, q_y, q_z, \\ m_{xxx}, m_{yyy}, m_{xxy}, m_{xyy}, m_{xyz}, m_{xxz}, m_{yyz} \end{bmatrix} \subset \text{R20 part}, \quad (25)$$

$$\Phi = \begin{bmatrix} \sigma_{xx}, \sigma_{yy}, \sigma_{xy}, \sigma_{xz}, \sigma_{yz}, \\ q_x, q_y, q_z, \\ m_{xxx}, m_{yyy}, m_{xxy}, m_{xyy}, m_{xyz}, m_{xxz}, m_{yyz}, \\ R_{xx}, R_{yy}, R_{xy}, R_{xz}, R_{yz}, \\ \Delta \end{bmatrix} \subset \text{R26 part}. \quad (26)$$

We have run the test cases for all of the parts of the module. However, as can be seen, the R13 and R20 equations are subsets of the R26 part and we will mainly focus on the validation cases of the R26 part in the report for simplicity.

5. Validation

Different types of geometry were used to test the implementation. Two-dimensional planar or curved surface and three-dimensional surface were adopted in the examples presented in the following subsections.

5.1 Channel Poiseuille flow

All the parts of the module are first tested for channel Poiseuille flows at different Knudsen numbers against the results of our in-house code, THOR, which is a 2-D multi-block parallel high-order moment equation solver. The channel configuration is shown in figure 2. The channel has a length of L and width of H . A gas with a mean velocity of u_m goes through the channel. The velocity profiles at $L/2$ are compared with the corresponding solutions from THOR, as shown in figure 3. The agreement between the two codes is excellent for all four newly added implementation: (a) NSF with slip; (b) the R13; (c) the R20 and (d) the R26 moment equations.

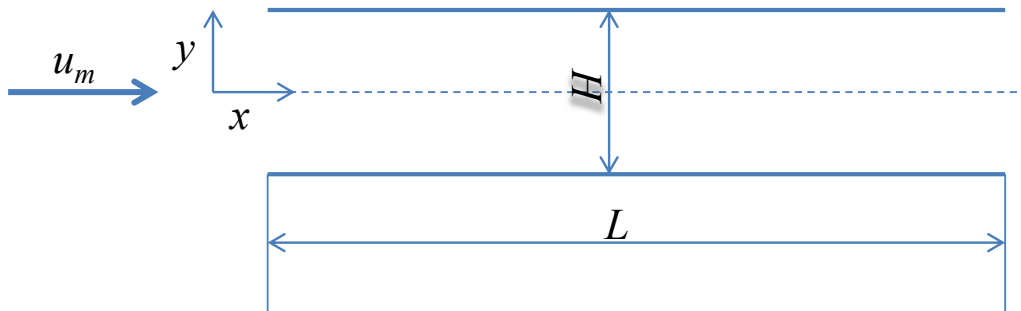


Figure 2 Channel flow configuration

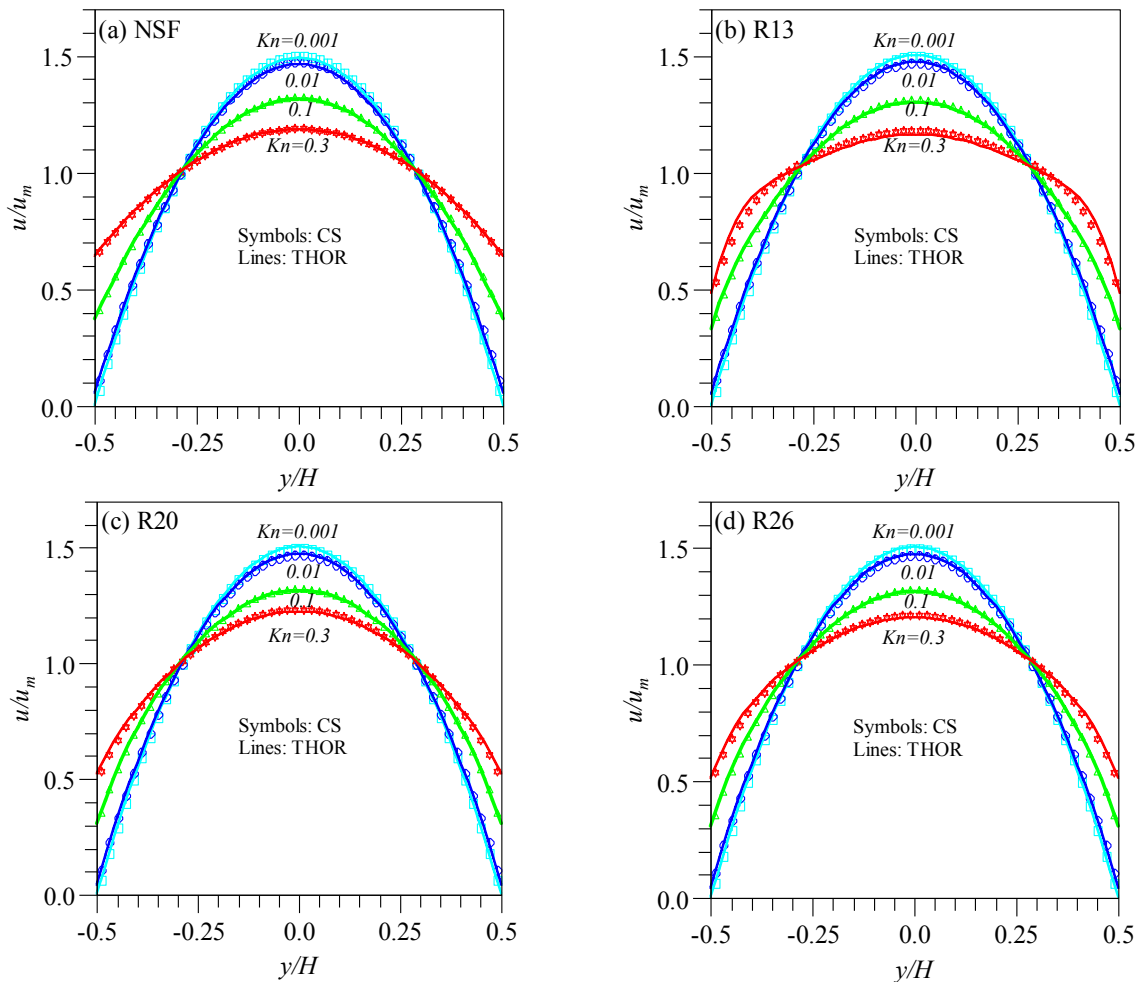


Figure 3 Comparison between THOR and *Code_Saturne* (CS). Velocity profiles for channel Poiseuille flows at different Knudsen numbers

5.2 Driven Cavity Flow

A rarefied gas flow of $Kn=0.5$ in a square driven cavity with a length of L is computed with all four parts of the module. The results from the R26 part are shown in figure 4, and compared with the data from the solution of the Boltzmann equation (BE) with the discrete velocity method (DVM). The profile of the velocity, U , along the y direction through the cavity centre is in good agreement with the BE-DVM solution, as indicated in figure 4(a). However, the R26 moment equations underpredict the velocity, V , along the x direction through the cavity centre in comparison with the BE-DVM solution. The discrepancy between the R26 and BE-DVM solutions is largely due to the limitation of the macroscopic models rather than the implementation of the moment method in *Code_Saturne*.

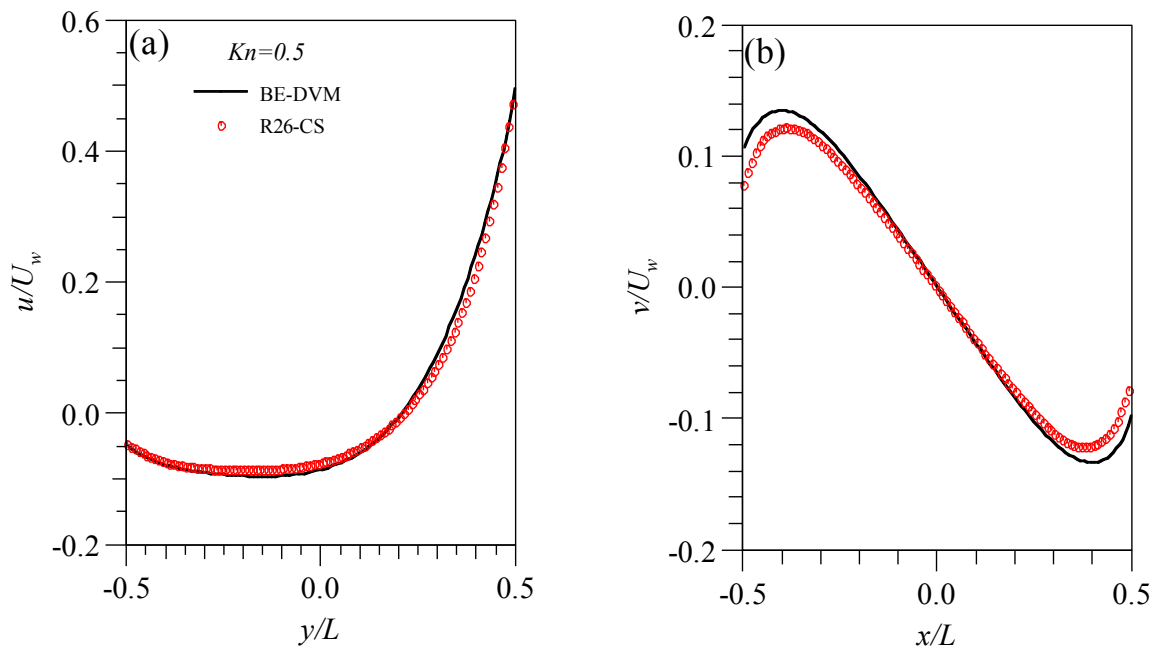


Figure 4 Velocity profiles along the lines through the cavity centre

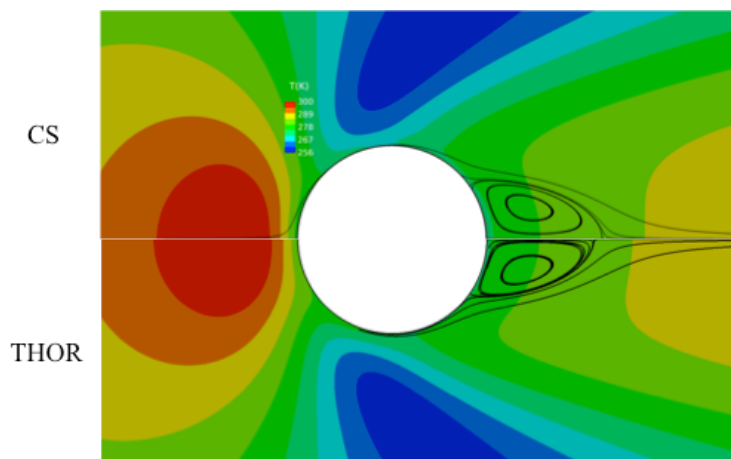


Figure 5 Flow past a circular cylinder. Streamlines and temperature field for $Kn=0.05$ and $Re=20$.
Top half : *Code_Saturne*; Bottom half: THOR

5.3 Flow past a circular stationary cylinder

The flow past a circular cylinder is computed with *Code_Saturne* to test the capability of the new added module over a curved surface. A structured grid is used around the cylinder and a triangular mesh is employed far away from the cylinder. At the inlet, outlet and side, symmetrical boundaries using a structured grid is used to satisfy the boundary conditions required by *Code_Saturne*. A total of 180,400 cells are used. Flows with a range of Reynolds number and Knudsen number are simulated. The vortex length predicted by the R26 module in *Code_Saturne* is slightly longer than that determined by THOR (Gu *et al.* 2019), as shown in figure 5 for $Kn=0.05$ and $Re=20$. However, both codes predict the thermal field well. The difference in the results might be explained by the fact that the added module is coupled with the incompressible solver in *Code_Saturne*, while the Mach number for this problem is greater than 0.6 and compressibility is important. The relationship between Re , Kn and Ma is (Gu *et al.* 2019):

$$Ma = \sqrt{\frac{2}{\gamma\pi}} Re Kn. \quad (27)$$

It can be seen from eq. (27) than Ma is proportional to the product of Re and Kn . When the gas departs from the continuum state, i.e. $Kn \gg 0$, the Reynolds number effect on the compressibility of the gas increases significantly. In the future, it is important to couple the added module with the compressible pressure solver. To do so, the energy equation, rather than the temperature field, given by equation (3), needs to be solved. New wall boundary conditions are required for the energy equation, but this was beyond the scope of the current project. This feature needs developing in the future.

5.4 Flow past a sphere

The flow past a sphere is computed with *Code_Saturne* for several Knudsen numbers in the slip regime to test the capability of the new added module over a three-dimensional curved solid surface. A structured grid is used around the sphere and triangular meshing employed far away from the sphere. Again, a structured grid is used for the boundary conditions at the inlet, outlet and side symmetrical boundaries, as required by *Code_Saturne*. A total of 7,135,116 cells are created. Shown in figure 6 is the relative pressure distribution around the sphere for $Kn=0.01$ and $Re=50$, predicted by *Code_Saturne's* R26 moment method. At the front of the sphere, the gas is compressed as the pressure raises above the free stream value. The gas expands as it passes the sphere and the local pressure is lower than the free stream pressure. As a result, a three-dimensional vortex ring is created behind the sphere, as shown in figure 7. It is worth noting that this is the very first time this type of simulation is possible.

Relative Pressure (Pa)

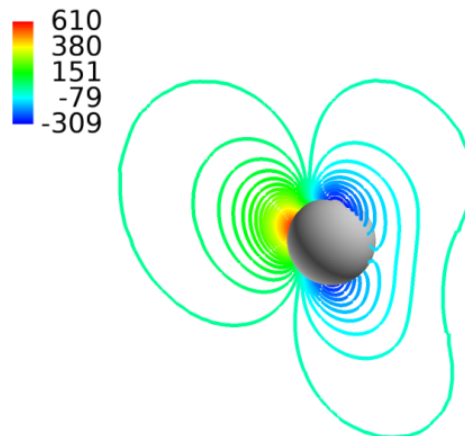


Figure 6 Relative pressure distributions in the vertical plane of a gas past a sphere. $Kn=0.01$ and $Re=50$

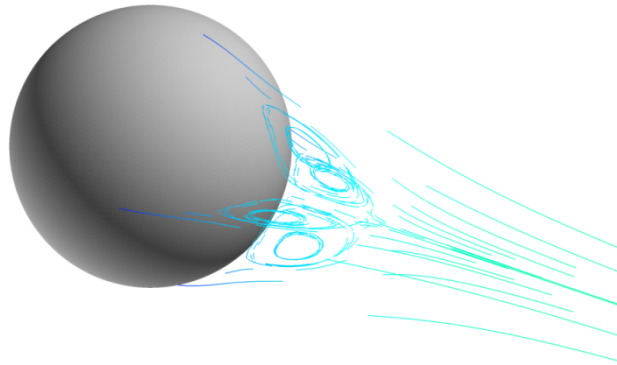


Figure 7 A vortex ring behind a sphere. $Kn=0.01$ and $Re=50$

5.5 Flow in porous media

To test the added module for a highly complex geometry, the flow past a cluster of randomly distributed cylinders is computed. This type of configuration is often used to study the permeability of porous media. The geometry shown in figure 8 has been provided by the University of Strathclyde. To calculate the wall boundary conditions, several layers of prisms/hexahedral cells, mimicking a structured grid are required around each cylinder. The velocity vectors shown in figure 8 indicate that the gas finds its optimal path through the porous media depending on the width of the gap between each cylinder. The velocity profiles at the exit and middle of the computational domain, as indicated in figure 8, are presented in figure 9. They are very close to the values obtained by the University of Strathclyde using kinetic theory.

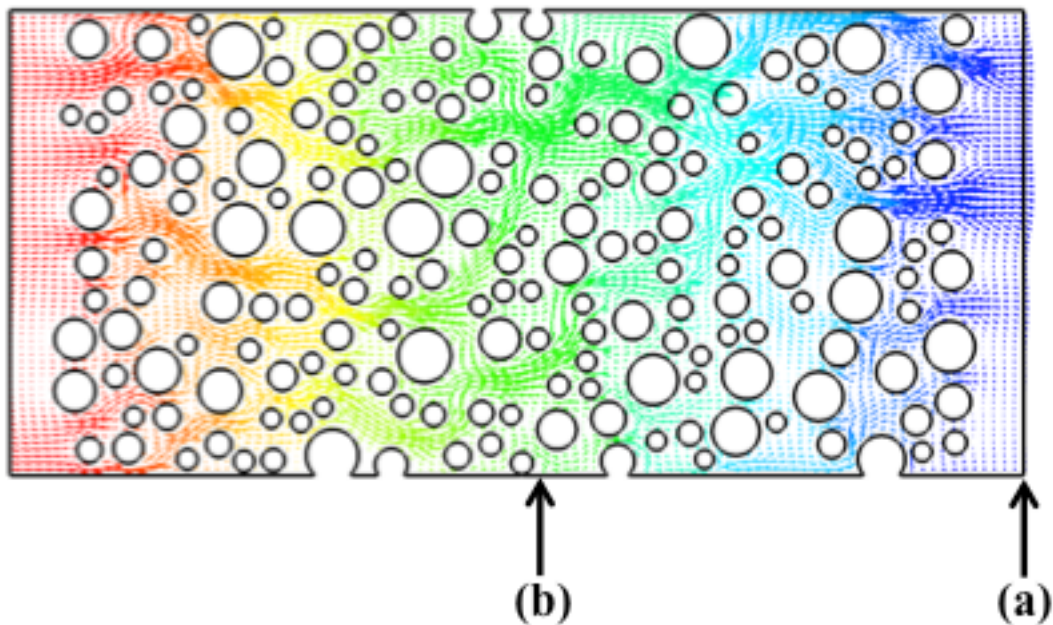


Figure 8 Velocity vectors of the gas through a cluster of randomly distributed cylinders

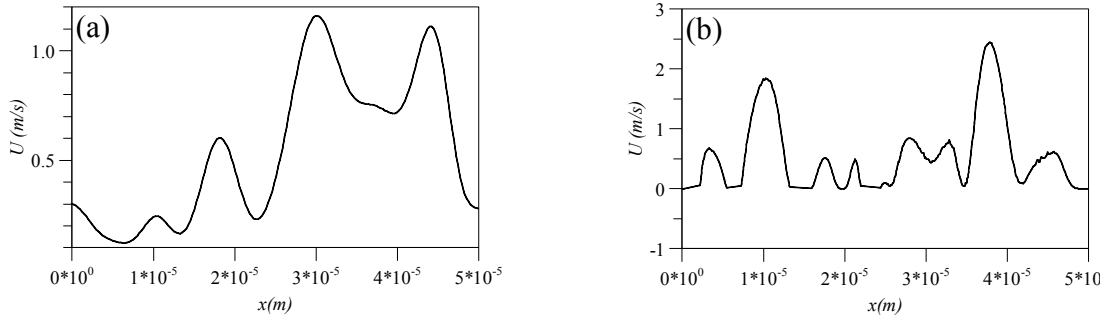


Figure 9 Velocity profiles at the exit and middle of the computational domain

5.6 Scalability of *Code_Saturne* with the new module

The scalability of the code with the added module is measured using the case of the flow past a sphere, in which 7,135,116 cells are used. The timing obtained on one node of ARCHER with 24 cores is adopted as the base in the calculation of the speedup shown in figure 10. Compared with the ideal speedup, the case using NSF with the slip boundary condition has a linear scaling up to 20 nodes. The performance deteriorates when more than 20 nodes are used for this case. The linear scaling goes up to 50 nodes for the R13 case. Interestingly, the R26 case has a super-linear scaling when less than 80 nodes are used. When more than 80 nodes are used, the speedup begins to drop as the number of cells in one node is reduced and the communication among the cores increases.

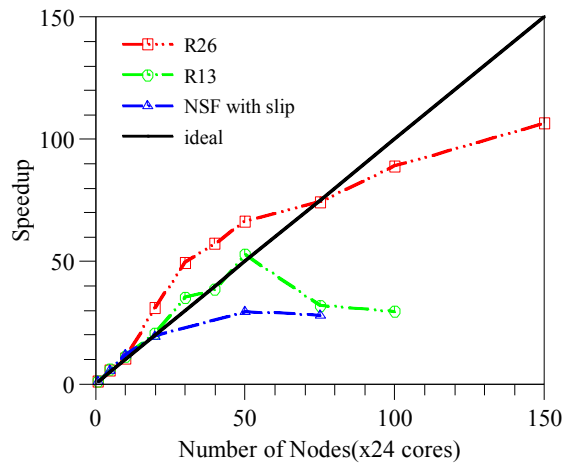


Figure 10 Speedup of the non-equilibrium gas flow module on ARCHER

6. Conclusions

The capability of the open-source CFD code, *Code_Saturne*, has been extended to simulate non-equilibrium gas flow by adding four modules based on the Method of Moments. The Cartesian components of the higher rank moments are solved as primary variables. The user subroutine facility has been utilised to implement the additional equations. The newly added module has been tested for two- and three-dimensional geometries with both planar and curved solid surfaces: (i) a regular channel configuration; (ii) the flow past an infinite circular cylinder (2-D); (iii) the flow past a sphere (3-D). The cases have been validated against available data to ensure the accuracy of the implementation. All the subroutines have been made available to the *Code_Saturne* development team in EDF R&D in order to make them part of the official release of the code. The new 3-D module, developed for massively parallel computers opens up many new areas of physics. For instance, some future work that could enhance the capabilities of this new module would include coupling to the compressible solver to handle flows with higher Mach numbers. Other features that would broaden the impact of the work could be the introduction of physics associated with evaporation.

Acknowledgement

This work is funded under the embedded CSE programme of the ARCHER UK National Supercomputing Service (<http://www.archer.ac.uk>). Thanks are given to Erwan Le Coupanec and Yvan Fournier (EDF), Alex Skillen, Greg Cartland-Glover and Stefano Rolfo (STFC Daresbury Laboratory) for their help during the implementation of the new module in *Code_Saturne*.

References

- CERCIGNANI, C. 1975 *Theory and Application of the Boltzmann Equation*. Scottish Academic Press, Edinburgh.
- CHAPMAN, S. & COWLING, T. G. 1970 *The Mathematical Theory of Non-uniform Gases*. Cambridge University Press.
- GAD-EL-HAK, M. 1999 The fluid mechanics of microdevices – The Freeman scholar lecture. *J. Fluids Eng.* **121**, 5-33.
- GRAD, H. 1949 On the kinetic theory of rarefied gases. *Commun. Pure Appl. Math.* **2**, 331-407.
- GU, X. J. & EMERSON, D. R. 2007 A computational strategy for the regularized 13 moment equations with enhanced wall-boundary conditions. *J. Comp. Phys.* **225**, 263-283.
- GU, X. J. & EMERSON, D. R. 2009 A high-order moment approach for capturing non-equilibrium phenomena in the transition regime. *J. Fluid Mech.* **636**, 177-216.
- GU, X. J., JOHN, B., TANG, G. H. & EMERSON, D. R. 2009 Heat and mass transfer of a rarefied gas in a driven micro-cavity. In: Proceedings of MNHMT09, MNHMT2009-18236.
- GU, X. J., EMERSON, D. R. & TANG, G. H. 2010 Analysis of the slip coefficient and defect velocity in the Knudsen layer of a rarefied gas using the linearized moment equations. *Phys. Rev. E* **81**, 016313, 2010.
- GU, X. J. & EMERSON, D. R. 2014 Linearized-moment analysis of the temperature jump and temperature defect in the Knudsen layer of a rarefied gas. *Phys. Rev. E* **89**, 063020.
- GU, X. J., BARBER, R.W., JOHN, B. & EMERSON, D. R. 2019 Non-equilibrium effects on flow past a circular cylinder in the slip and early transition regime. *J. Fluid Mech.* **860**, 654-681.
- MAXWELL, J. C. 1879 On stresses in rarified gases arising from inequalities of temperature. *Phil. Trans. Roy. Soc. (Lond.)* **170**, 231-256.
- STRUCHTRUP, H. 2005 *Macroscopic Transport Equations for Rarefied Gas Flows*. Springer-Verlag, Berlin Heidelberg.
- STRUCHTRUP, H. & TORRILHON, M. 2003 Regularization of Grad's 13 moment equations: Derivation and linear analysis. *Phys. Fluids* **15**, 2668-2680.
- TAHERI, P. and STRUCHTRUP, H. 2009 Effects of rarefaction in microflows between coaxial cylinders. *Phys. Rev. E* **80**, 066317.
- TAHERI, P., TORRILHON, M. and STRUCHTRUP, H. 2009 Couette and Poiseuille microflows: Analytical solutions for regularized 13-moment equations. *Phys. Fluids* **21**, 017102.
- TAHERI, P. & STRUCHTRUP, H. 2010 An extended macroscopic transport model for rarefied gas flows in long capillaries with circular cross section. *Phys. Fluids* **22**, 112004.
- YOUNG, J. B., Calculation of Knudsen layers and jump conditions using the linearised G13 and R13 moment methods 2011 *Int. J. of Heat and Mass Transfer* **54**, 2902-2912.